Preprint No. 2021-02

Combined ANN-FEM approach for spatial-temporal structural response prediction: Method and experimental validation

M. Drieschner*[1], C. Wolf[1], F. Seiffarth[1], Y. Petryna[1]

October 21, 2021

*Correspondence: M. Drieschner: martin.drieschner@tu-berlin.de
[1]Technische Universität Berlin, Faculty VI Planning Building Environment, Department of Civil Engineering, Chair of Structural Mechanics, Gustav-Meyer-Allee 25, 13355 Berlin, Germany

Suggested Citation: M. Drieschner, C. Wolf, F. Seiffarth, Y. Petryna. Combined ANN-FEM approach for spatial-temporal structural response prediction: Method and experimental validation. *Preprint-Reihe des Fachgebiets Statik und Dynamik, Technische Universität Berlin*, Preprint No. 2021-02, 2021. http://dx.doi.org/10.14279/depositonce-12508.

Preprint-Reihe des Fachgebiets Statik und Dynamik, Technische Universität Berlin auf https://depositonce.tu-berlin.de/

Combined ANN-FEM approach for spatial-temporal structural response prediction: Method and experimental validation

M. Drieschner, C. Wolf, F. Seiffarth, Y. Petryna

Abstract

The prediction of system outcomes like strains or displacement fields in real technical systems is demanding due to the presence of unavoidable uncertainties. These uncertainties should be considered, for example by different uncertainty models either based on probabilistic, possibilistic or other approaches. In this contribution, a non-linear stability analysis of a three-dimensional carbon fiber reinforced plastic (CFRP) considering aleatory and epistemic uncertainties is conducted. For the realistic incorporation of the uncertainties in the finite element model, thickness variations and geometrical inaccuracies have been detected in advance by non-destructive testing on a real structure made of CFRP. Additionally, the material parameters have been defined as stochastic variables based on reference studies in the literature. If the underlying deterministic model itself is also time-consuming, it can be useful to surrogate the overall numerical simulation. Strains and displacement fields have been measured in a symmetric three-point bending test and compared to the numerical predictions produced by artificial neural networks (ANN). A sensitivity analysis is finally conducted which clarifies the strong dependence of the outcomes on the fiber volume content, the structural thicknesses and the stiffness in fiber direction.

Keywords *aleatory uncertainty; epistemic uncertainty; artificial neural networks (ANN); carbon fiber reinforced plastic (CFRP); global stability failure*

1 Introduction

The failure analysis of real structures is a challenge which can be conducted in two ways: experimentally or numerically. Real experiments are mostly displacement-controlled and for each measurement step, the applied load, displacements and strains can be recorded by appropriate technical devices. Load-displacement or load-strain curves can exemplarily be extracted from the experimental values. In the numerical way, a non-linear analysis using the incremental-iterative Newton-Raphson method [2] is usual obtaining load-dependent system outcomes. A non-linear simulation can be time-consuming, especially in the presence of uncertainties which should be considered in the input variables. The analysis on a real structure should clarify the use of surrogating the numerical simulation by comparing the achieved results also to the experimentally determined ones.

Therefore, the focus in this study is on the global stability failure of structural components made of carbon fiber reinforced plastic (CFRP). This failure mechanism can occur of thin-walled spatial structures, e.g. of rotor blade components of wind turbines in operation for which special investigations are mandatory in the design process [3]. On a representative thin-walled structure, experimental and numerical studies have been conducted like in [17, 31]. It is assumed that the stability failure is mainly affected by material imperfections and geometrical inaccuracies [10]. Both are unavoidable due to partly hand-made manufacturing processes and have to be incorporated in the underlying finite element model. The scattering of material parameters affects the structural stiffness and consequently the system outcomes like strains and stresses [30]. The influence of geometrical inaccuracies on the stability failure of thin-walled structures has been numerically evaluated in [5]. As a drawback, the non-linear analysis in the

presence of the mentioned uncertainties is highly time-consuming. Therefore, Artificial Neural Networks (ANNs) [12] can efficiently work as a forecast surrogate to predict spatial-temporal system outcomes [4, 35]. The successful application of ANNs as surrogate forecast model and its variants like Convolutional Neural Networks for image classification and Recurrent Neural Networks for audio recognition has been demonstrated extensively, e.g. in [12, 19]. Among the vast of literature, a systematic introduction is given in [26]. Especially regarding engineering applications, the conference proceedings [24] and the book [1] present current trends for the solution of complex engineering problems. In the field of uncertainty quantification, neural networks have been used with fuzzy data in [14] and with polymorphic uncertain data in [13, 11].

The remainder of this paper is organized as follows: The structure, called omega shell supported by steel profiles and by a plate made of glass fiber reinforced plastic (GFRP), is described in detail in Section 2. Section 3 provides first the measurements of the geometrical inaccuracies in advance of and, secondly, the experimental setup during the symmetric three-point bending test. Due to different uncertainty sources and knowledge about the present uncertainties, a distinction in aleatory and epistemic uncertainties [18] with different uncertainty models is suggested as described in Section 4. The numerical results, their comparison with experimental results and a sensitivity analysis are presented in Section 5. Finally, some concluding remarks are given in Section 6.

2 Omega shell

In order to observe the influence of material and geometrical uncertainties on a numerically demanding problem, a structural component, a measurement procedure and an experimental routine have been designed and implemented. Elastic buckling of a CFRP structure has been chosen, since it is strongly dependent on various uncertainties, especially the geometrical imperfections (e.g. wall thickness). In order to design an appropriate setup, fulfilling certain conditions is important, for example an easy and cost-effective manufacturing incorporating CFRP materials, the possibility to observe buckling with optical measurement devices and creating a designated area for the buckles to form. The proposed structure, see Fig. 1, is a folded structure with an Ω-shaped cross-section and thin-walled, tilted webs (referred to as A and B). It is 1.20 m long, 0.88 m wide, 0.40 m high and designed to ensure that the first buckling modes occur dominantly within the tilted webs. These are about half as thin as the remaining flanges (buckling strength is proportional to the third power of the wall thickness [10]) and dominantly undergo compressive stress in a symmetric three-point bending test. In a first iteration, a quasi-isotropic laminate layering with a fiber volume content of $\varphi_{\mathrm{des}} = 55\,\%$ has been chosen, consisting of a $[0°/45°/90°/-45°]_{\mathrm{S}}$ set-up for the webs and twice the amount for the flanges, yielding a web thickness of $t_{\mathrm{w}} = 3.33\,\mathrm{mm}$ and a flange thickness of $t_{\mathrm{f}} = 6.66\,\mathrm{mm}$. The design has been made in cooperation with IPF Dresden (https://www.ipfdd.de). As a local partner, they also friendly undertook the manufacturing. The calculated mass for the whole CFRP structure (without GFRP plate and edge reinforcements) is $m_{\mathrm{des}} = 9.49\,\mathrm{kg}$. The mean values ($\bar{\bullet}$) of the relevant mechanical properties of the carbon fibers (Tenax STS40 F13 F24K 1600tex from Teijin Carbon Europe GmbH [29]) and of the matrix material (EPL 20 epoxy resin and EPH 161 hardener from R&G Faserverbundwerkstoffe GmbH [25]) are presented in Table 1.

The finished composite shell structure is presented in Fig. 2a. To prevent premature buckling of the whole structure due to the free edges of the tilted webs, they are strengthened using specially designed edge supports made of steel U-profiles, see Fig. 2b for reference. They can seamlessly slide onto the free edges.

The open cross-section tends to spread wide open in x-direction during the load application in the test setup. A GFRP plate with high in-plane stiffness is glued in advance to the bottom of the structure to eliminate this problem.

Table 1: Mechanical properties of fibers (f) and matrix (m) material

Fibers (f)	Matrix (m)
$\bar{E}_{\parallel \mathrm{f}} = 238\,000\,\mathrm{MPa}$	$\bar{E}_{\mathrm{m}} = 3150\,\mathrm{MPa}$
$\bar{E}_{\perp \mathrm{f}} = 16\,000\,\mathrm{MPa}$	
$\bar{G}_{\perp\parallel \mathrm{f}} = 50\,000\,\mathrm{MPa}$	$\bar{G}_{\mathrm{m}} = 1150\,\mathrm{MPa}$
$\bar{\nu}_{\perp\parallel \mathrm{f}} = 0.270$	$\bar{\nu}_{\mathrm{m}} = \bar{E}_{\mathrm{m}} / \left(2\bar{G}_{\mathrm{m}}\right) - 1 = 0.370$
$\bar{\varrho}_{\mathrm{f}} = 1770\,\mathrm{kg\,m^{-3}}$	$\bar{\varrho}_{\mathrm{m}} = 1190\,\mathrm{kg\,m^{-3}}$

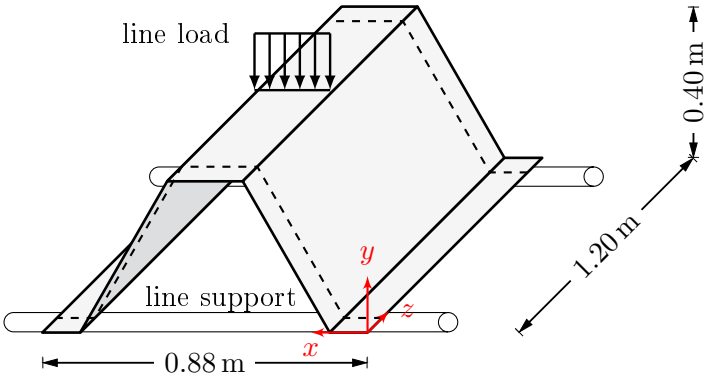

Figure 1: CFRP structure with load and support

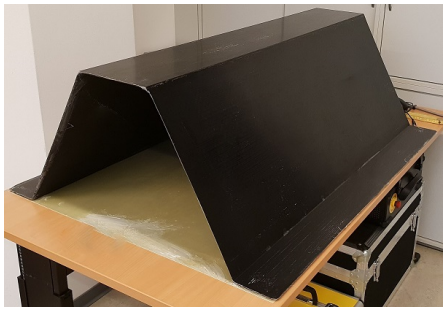

(a) Assembled CFRP structure with GFRP plate

(b) Steel reinforcements to support both free edges against premature buckling

Figure 2: Omega shell and edge reinforcement

3 Measurements and experimental setup

After finishing the manufacturing process, an initial inspection of the omega shell has been carried out. Particularly noteworthy is the rather smooth and even surface on the outside, while the inside one is more uneven and bumpy. The true weight of the structure (without GFRP plate and edge reinforcements) is $m_{\mathrm{true}} = 10.78\,\mathrm{kg}$. Since the mass of fibers within the matrix is fixed one can recalculate the true fiber volume content to $\varphi_{\mathrm{true}} = 47\,\%$.

In advance of the symmetric three-point bending test, the geometrical imperfections, namely web thicknesses (Section 3.1) and dimensional deviations of the overall geometry (Section 3.2), have been measured since they have a significant influence on the buckling behavior [10]. Other imperfections, like material or physical imperfections (for example air voids within the matrix, initial cracks, variation of material parameters) have not been measured. Nonetheless, they also tend to have an impact on the buckling behavior, see Section 5.

During the test, an experimental setup enables the continuous measurement of loads, strains

and displacements, see Section 3.3.

3.1 Web thickness measurement using pulse-echo method

As previously mentioned, the inside surface of the omega shell is not smooth and rather uneven up to a certain degree due to the manufacturing process. Since the web thickness is only a few millimeters, even small variations can have a meaningful influence on the buckling behavior. The actual thickness measurements have been performed using the ultrasonic pulse-echo system *MUSE Z-400*. Both web areas have been scanned with a minimum resolution of 150 µm resulting in over 44 million data points per square meter. The overall results are displayed in Fig. 3, where

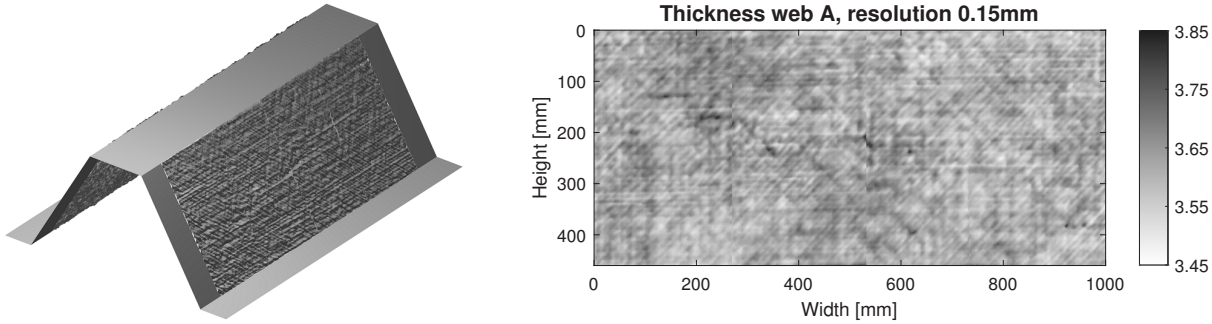

(a) Measured web thickness on web A and B amplified by a factor of 50

(b) Thickness distribution of web A in millimeters

Figure 3: Ultrasonic measurement of the web thickness

the thickness of the webs is amplified by a factor of 50. Due to some mounting limitations of the measurement device, it has not been possible to cover the remaining 10 cm in front of every web edge. The mean thickness of both webs $\mu_{\text{true}} \approx 3.61\,\text{mm}$ is about 8 % larger than the designed thickness $t_{\text{des}} = 3.33\,\text{mm}$.

3.2 Global geometry measurement using fringe projection method

An optical measurement using the fringe projection method has been used to get information about the actual shape of the structure. Here, a specific pattern of different fringes is projected onto an object and measured using a calibrated camera. After applying data processing techniques, the results are presented as triangular mesh of the geometry. This data can be analyzed further or compared to the designed geometry. The deviation of the real geometry from the design is presented in Fig. 4. The numbers indicate the deviation from the perfect geometry in

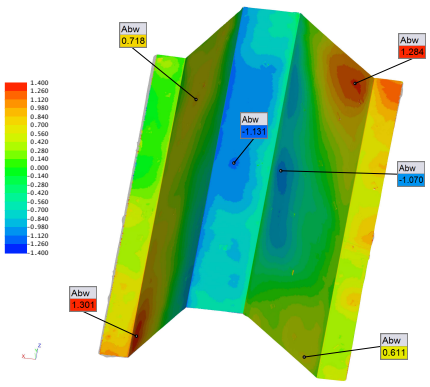

Figure 4: Deviations from design geometry in millimeters

millimeters, where positive numbers represent an outward shift, whereas negative numbers repre-

sent an inward shift. First of all, the overall deviation from the perfect geometry is comparatively small with a maximum positive shift of 1.3 mm and a minimum negative shift of 1.1 mm based on the overall dimensions of the structure. It implies that the manufacturing did not introduce major geometry deviations. Nonetheless, there still are deviations, especially within the webs which may influence the buckling behavior to a certain degree.

3.3 Experimental setup

The main objective of the experimental setup is to induce structural buckling and to observe corresponding deformations/strains on the surface of both webs, while also recording the applied displacement and the associated load. Three strain gauges have been applied to measure the strains on web B, see Fig. 5a. The strain gauges 1 and 2 have been attached in the middle of web B to measure horizontal and vertical strains and strain gauge 3 has been attached at the bottom flange to measure horizontal strains. Web A has been prepared with a black and white random pattern to use a stereo optic camera system for non-contact deformation and strain measurement of the whole web area over the entire time. The test setup is displayed in Fig. 5b.

The experiment has been conducted displacement-controlled with a constant rate of 500 µm/ min. This way it is possible to observe the post-buckling behavior of the structure, in case the structure is loosing stiffness on a certain path. The whole test has lasted about 30 min including some short interruptions. The structure has violently failed at a vertical load of 45.36 kN and a vertical displacement of 11.62 mm with an abrupt crack formation on the inside of the bottom of the upper flange. It has clearly been visible during the test that the structure has buckled almost symmetrically with major deformations on both webs.

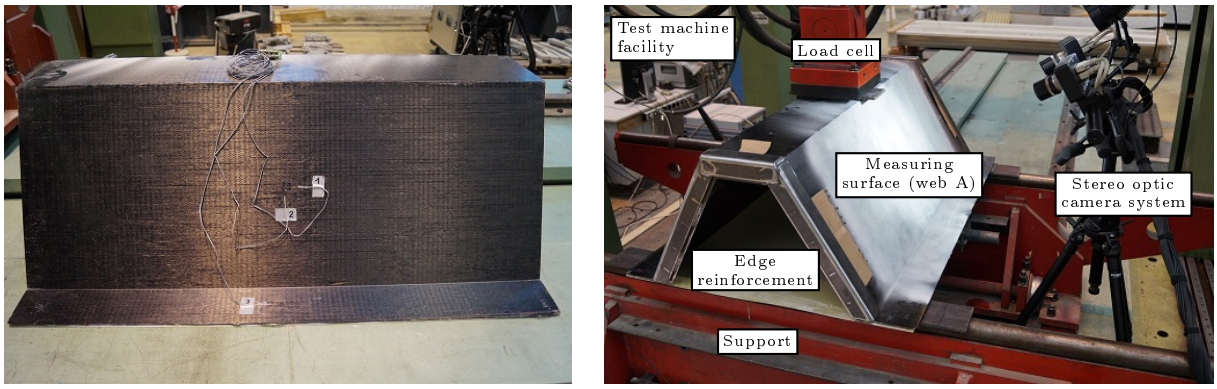

(a) Strain gauge arrangement (1: web B horizontal, 2: web B vertical, 3: flange horizontal)

(b) Operational test setup with stereo optic camera system for deformation/strain measurement on web A

Figure 5: Strain gauge arrangement and test setup overview

4 Uncertainty models

Various uncertainties in the material and geometrical properties are present and have to be considered in the numerical investigations. Some of them are irreducible due to randomness and natural variability. Statistical information are at disposal in the literature or from conducted non-destructive testing. These uncertainties are called aleatory [18] and are quantified by random variables. In this study, lognormal distributions $\mathcal{LN}(\mu, \sigma)$ with μ as mean value of logarithmic values and σ as standard deviation of logarithmic values are used for all random variables, see Fig. 6a. Some uncertain parameters are based on limited amount of data, subjectivity or expert knowledge and no statistical information is given which could reduce the uncertainty. These uncertainties are called epistemic [18] and can be quantified by non-stochastic variables [22].

In this study, fuzzy variables with a triangular membership function, called triangular fuzzy numbers TFN$\langle a, b, c\rangle$, with support $[a, c]$ and core value b are used, see Fig. 6b [15].

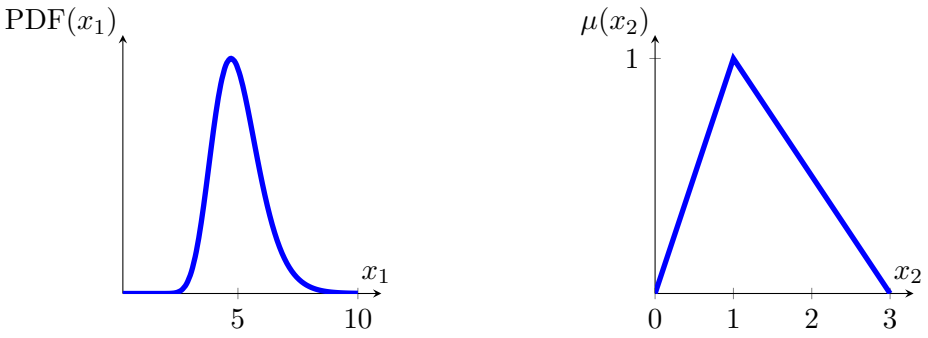

(a) Lognormal distribution: $x_1 \sim \mathcal{LN}(\mu = 5, \sigma = 1)$

(b) Triangular fuzzy number: $x_2 = \mathrm{TFN}\langle a = 0, b = 1, c = 3\rangle$

Figure 6: Uncertainty models

In Section 4.1, uncertainty models for the material parameters are defined. In Section 4.2 and 4.3, the measurement data from Section 3.1 and 3.2, respectively, are used to define further uncertain variables. Finally, a large uncertainty is given for the edge support area, which is discussed in Section 4.4.

4.1 Material parameters

The omega shell is made of carbon fiber reinforced plastic (CFRP) which is a multilayer composite consisting of individual unidirectional fiber layers. For each of them, transverse isotropy is assumed. The material parameters depends on the fiber (f) [29] and matrix (m) [25] properties which have been experimentally determined [33]. The mean values from Table 1 are used, together with a coefficient of variation (COV) of 5 % [34], see Table 2.

Table 2: Uncertain material parameters of fibers (f) and matrix (m) material

	Fibers (f)		Matrix (m)
$E_{\parallel \mathrm{f}} \sim$	$\mathcal{LN}(238000, 11900)$ MPa	$E_{\mathrm{m}} \sim$	$\mathcal{LN}(3150, 157.5)$ MPa
$E_{\perp \mathrm{f}} \sim$	$\mathcal{LN}(16000, 800)$ MPa		
$G_{\perp\parallel \mathrm{f}} \sim$	$\mathcal{LN}(50000, 2500)$ MPa	$G_{\mathrm{m}} \sim$	$\mathcal{LN}(1150, 57.5)$ MPa
$\nu_{\perp\parallel \mathrm{f}} \sim$	$\mathcal{LN}(0.270, 0.0135)$		
$\varrho_{\mathrm{f}} \sim$	$\mathcal{LN}(1770, 88.5)\,\mathrm{kg\,m^{-3}}$	$\varrho_{\mathrm{m}} \sim$	$\mathcal{LN}(1190, 59.5)\,\mathrm{kg\,m^{-3}}$

Based on [28], the material parameters $E_\parallel$, $E_\perp$, $\nu_{\perp\parallel}$ and $G_{\perp\parallel}$ and further dependent material parameters $\nu_{\parallel\perp}$, $\nu_{\perp\perp}$ and $G_{\perp\perp}$ of the unidirectional layer can be calculated in dependence of the fiber volume content φ. The influence of a reduction of $E_\perp$ and $G_{\perp\parallel}$ on the results caused by material non-linear effects [16, 7] has been investigated. Only small deviations have been observed, so the material non-linearity is negligible and has been excluded in the following.

Inaccuracies in the manufacturing lead to imperfect undulated unidirectional layers. The undulation is considered by reducing the stiffness in longitudinal direction $E_\parallel$ for which a factor $r_\parallel \approx 90\,\%$ is usual [33]. In the following, the fuzzy variable $r_\parallel = \mathrm{TFN}\langle 80, 90, 95\rangle\,\%$ is defined.

4.2 Web thickness

The design thickness is $t_{\mathrm{des}} = 3.33\,\mathrm{mm}$ for both webs (A and B). It could be measured by ultrasonic scanning, see Fig. 3, that the real thickness is spatially varying and about 8 % larger. All measured thicknesses are displayed in a histogram, see Fig. 7. The mean value for both webs is $\mu_{\mathrm{true}} \approx 3.61\,\mathrm{mm}$ and the COV is around 1 %. Based on that, a lognormal distribution for the web thickness $t_{\mathrm{w}} \sim \mathcal{LN}\,(3.61, 0.0361)\,\mathrm{mm}$ has been defined. It is worth mentioning that the increase of the mean value is more important for the stability analysis of the webs than the small spatial deviations. Thus, a spatially constant thickness t_{w} has been defined in this study. An extension to a (fuzzy-)random field definition [27] is possible and can be considered in ongoing studies.

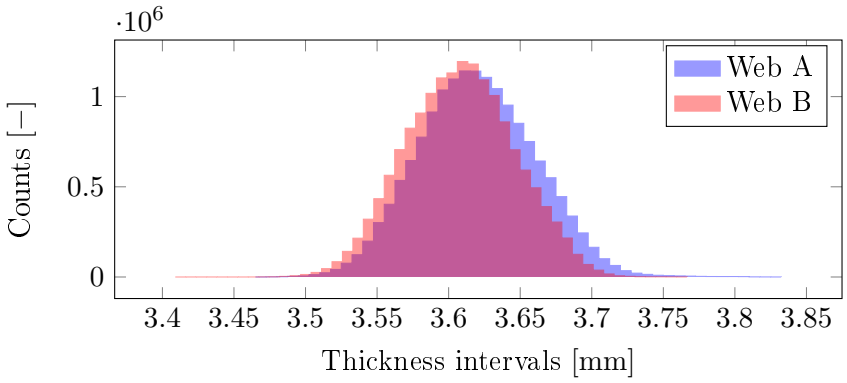

Figure 7: Web thickness: histogram of measurement data using a measurement resolution of 150 µm

4.3 Global geometry deviation

In addition to the web thickness, the global geometry has been measured and deviations from the original design could been determined, see Fig. 4. The deviations are considered in two different ways.

On the one hand, triangular fuzzy numbers are defined for the offsets of the web edges and the upper flange which are probably caused by "spring-in effects" in the manufacturing process [33]. Two opposite web edges have an offset of $\approx 1.3\,\mathrm{mm}$, the other ones of $\approx 0.7\,\mathrm{mm}$ and the upper flange of $\approx 1.1\,\mathrm{mm}$. To investigate the influence of the offsets, triangular fuzzy numbers $\Delta_{\mathrm{wA}} = \mathrm{TFN}\langle 0, 0, 1.50\rangle\mathrm{mm}$, $\Delta_{\mathrm{wB}} = \mathrm{TFN}\langle 0, 0, 0.75\rangle\mathrm{mm}$ and $\Delta_{\mathrm{uf}} = \mathrm{TFN}\langle -1.50, 0, 0\rangle\mathrm{mm}$ are defined with no offset on the core and maximum offset on the support.

On the other hand, the initial deformation of the web surfaces has been considered by an imperfect pre-deformed geometry according to the symmetrical buckling mode. No value for the maximum deflection u_{imp} can explicitly be given, so a case study has been conducted in a range of $u_{\mathrm{imp}} \in [0.00, 10.00]\,\mathrm{mm}$.

4.4 Edge support area

The omega shell has been reinforced on both longitudinal edges by steel U-profiles, see Section 2. For both webs (A and B) and the upper flange, the length of the support area is uncertain. It is assumed, that the reinforcement has an effect at least between 30 % and 70 % of the length. The maximum range has been specified between 5 % and 95 %. Each of the procentual start values a_{wA}, a_{wB} and a_{uf} is quantified by $a_\bullet = \mathrm{TFN}\langle 5, 30, 30\rangle\%$ and each of the procentual end values b_{wA}, b_{wB} and b_{uf} is quantified by $b_\bullet = \mathrm{TFN}\langle 70, 70, 95\rangle\%$.

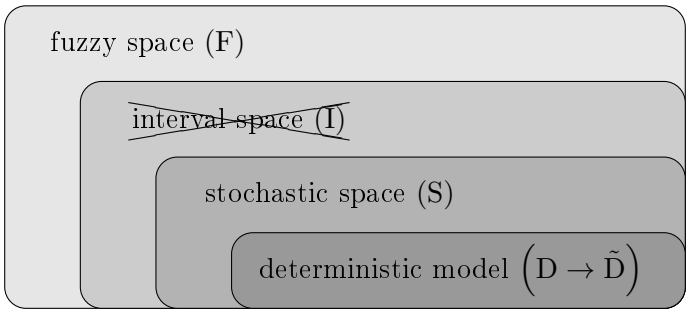

Figure 8: General scheme of a nested fuzzy-stochastic analysis

5 Results

Defining stochastic variables for aleatory uncertainties and fuzzy variables for epistemic uncertainties simultaneously leads to a nested fuzzy-stochastic analysis. The deterministic finite element model (D) is embedded in the uncertainty space, which generally consists of the stochastic space (S), the interval space (I) and the fuzzy space (F), see Fig. 8. In this approach, the interval space is empty and has not to be considered. It is usual that the stochastic space is embedded in the fuzzy space. The computational costs can be calculated as $t_{\mathrm{tot}} = n_{\mathrm{tot}} \cdot t_{\mathrm{D}} = n_{\mathrm{F}} \cdot n_{\mathrm{S}} \cdot t_{\mathrm{D}}$ with the number of samples in the fuzzy space n_{F}, the number of samples in the stochastic space n_{S} and the duration t_{D} of the non-linear stability analysis of the deterministic model. Since the deterministic model (D), created in the finite element program ANSYS, is very time-consuming ($t_{\mathrm{D}} \approx 3.5\,\mathrm{min}$), it is replaced by a surrogate model $\left(\mathrm{D} \to \tilde{\mathrm{D}}\right)$ by using artificial neural networks (ANNs).

Individual ANNs have been realized with the open source software Keras [6, 23] for each of the following outcomes: Strain $\epsilon_{1,\mathrm{z}}$, strain $\epsilon_{2,\mathrm{x}}$, strain $\epsilon_{3,\mathrm{z}}$, each measured by a strain gauge, and the displacement normal to the web surface in the center $u_{\mathrm{M,norm}}$. 10000 different samples of

$$\begin{aligned} \boldsymbol{p} \;=\; & \big(\varphi, E_{\parallel\mathrm{f}}, E_{\perp\mathrm{f}}, G_{\perp\parallel\mathrm{f}}, \nu_{\perp\parallel\mathrm{f}}, \varrho_{\mathrm{f}}, E_{\mathrm{m}}, G_{\mathrm{m}}, \varrho_{\mathrm{m}}, r_{\parallel}, \ldots \\ & t_{\mathrm{w}}, \Delta_{\mathrm{wA}}, \Delta_{\mathrm{wB}}, \Delta_{\mathrm{uf}}, u_{\mathrm{imp}}, a_{\mathrm{wA}}, a_{\mathrm{wB}}, a_{\mathrm{uf}}, b_{\mathrm{wA}}, b_{\mathrm{wB}}, b_{\mathrm{uf}}\big) \end{aligned} \tag{1}$$

have been created in advance, using 52 values for the vertical load $F_{\mathrm{z}} = F_{\mathrm{z}}(t)$ between 0 kN and 60 kN. 15% of them have been used for testing the network. The remaining 85% have been divided in 80% for training and 20% for validating the network [32]. For all ANNs, the Huber loss function with varying values for δ_{Huber} serves as objective function. The hyperband algorithm [21] and a following grid search [9] leads to "optimal" ANN parameters, some of them are given in Table 3. The quality of the individual predictions by ANN can be quantified by the training loss and validation loss values, also listed in Table 3. The surrogate $\left(\mathrm{D} \to \tilde{\mathrm{D}}\right)$ is assessed as reasonable.

The numerical prediction of the displacement field, measured by a stereo optic camera system, increases the ANN complexity by the spatial component $\boldsymbol{x}$. Two different approaches are pursued in the following:

idea 1 creating an ANN for a multidimensional output: $(\boldsymbol{p}, F_{\mathrm{z}}(t)) \mapsto \boldsymbol{u}_{\mathrm{norm}}(\boldsymbol{x})$

idea 2 defining the spatial component as ANN input: $(\boldsymbol{p}, F_{\mathrm{z}}(t), \boldsymbol{x}) \mapsto u_{\mathrm{norm}}(\boldsymbol{x})$

In the present case, idea 1 leads to an easier ANN architecture with less necessary neurons. Furthermore, the evaluation of the ANN based surrogate model for the overall displacement field is faster due to the definition of a multidimensional output $\boldsymbol{u}_{\mathrm{norm}}(\boldsymbol{x})$. In contrast to idea 1, the spatial component $\boldsymbol{x}$ is part of the ANN input in idea 2. Consequently, the architecture and the evaluation is more complex and more costly. But an advantage lies in the higher flexibility for

Table 3: Some determined "optimal" ANN parameters and ANN quality values

parameter	$\epsilon_{1,z}$	$\epsilon_{2,x}$	$\epsilon_{3,z}$	$u_{M,norm}$
δ_{Huber}	0.01	0.01	0.01	0.01
layers	2	2	4	3
neurons per layer	$2048 \to 512$	$1024 \to 1024$	$256 \to 1024 \to 2048 \to 2048$	$1024 \to 256 \to 512$
activation function	swish	relu	relu	swish
dropoutrate	0.5	0.5	0.3	0.0
optimizer	adam	nadam	adam	adam
training loss	$5.51 \cdot 10^{-3}$	$5.24 \cdot 10^{-3}$	$7.62 \cdot 10^{-3}$	$9.06 \cdot 10^{-6}$
validation loss	$2.23 \cdot 10^{-3}$	$4.71 \cdot 10^{-3}$	$5.65 \cdot 10^{-3}$	$6.55 \cdot 10^{-4}$

the evaluation in the spatial component $\boldsymbol{x}$. The deviation between both ideas is quite small, see Section 5.2.

Finally, the complete numerical analysis is conducted in MATLAB, mainly by using the framework PolyUQ [8]. In the fuzzy space, the reduced transformation method [15] by using a priori fuzzy input dependencies and additional 100 free samples on each of eleven equidistantly distributed α-levels are used. In the stochastic space, the classical Monte-Carlo method with $n_S = 1000$ samples on each fuzzy sample is conducted.

In Section 5.1 and 5.2, the experimental and numerical results for the horizontal strain $\epsilon_{1,z}$ at position 1 and for the displacement normal to the web $\boldsymbol{u}_{norm}(\boldsymbol{x})$ are presented. For the numerical investigations, three cases have been considered first:

case 1 $\varphi_{des} = 55\,\%$, perfect geometry

case 2 $\varphi_{true} = 47\,\%$, perfect geometry

case 3 $\varphi_{true} = 47\,\%$, pre-deformed geometry according to the symmetrical buckling mode with maximum deflection of $u_{imp} = \mu_{true} = 3.61\,\mathrm{mm}$ outward on both webs A and B

For all three cases, the mean value $\mu(\bullet)$ and the standard deviation $\sigma(\bullet)$ have been calculated in the stochastic space. For both, the membership functions $\mu(\mu(\bullet))$ and $\mu(\sigma(\bullet))$ can be shown and the center of gravity (COG) has been selected as defuzzified value [20] in the fuzzy space.

To visualize the most influential input parameters on the system outcomes, a sensitivity analysis is finally conducted in Section 5.3.

5.1 Strain gauge 1

The horizontal strain at position 1 has been measured experimentally with a maximum value of $1.52\,\mathrm{mm\,m^{-1}}$, see Fig. 9a and 9b. The reduction of the fiber volume content ϕ and the consideration of a pre-deformed geometry increase the fuzzy mean value of the horizontal strain $\epsilon_{1,z}$. The COG of the fuzzy mean value in all three cases is lower with a maximum value of $1.30\,\mathrm{mm\,m^{-1}}$ in case 3. The COG at the maximum load of $F_z(t) = -45.36\,\mathrm{kN}$ has been increased compared to the COG of case 1 ($\approx 0.77\,\mathrm{mm\,m^{-1}}$) by approximately 38 % for case 2 and 69 % for case 3, respectively. Furthermore, case 3 with the pre-deformed geometry is more appropriated to retrace the experimentally measured values. The experimental curve is completely inside the support of the fuzzy mean value (e.g. $1.52 \in [1.13, 1.54]\,\mathrm{mm\,m^{-1}}$ at $F_z(t) = -45.36\,\mathrm{kN}$), even the experimental curve becomes steeper for higher load values. The calculated fuzzy standard deviations of all three cases are comparable and are increasing by higher load values, see Fig. 9c. The rapid increase of the strain values in case 1 from approximately $F_z(t) = -17\,\mathrm{kN}$ and in case

2 from approximately $F_z(t) = -20\,\mathrm{kN}$ is also identifiable in the fuzzy standard deviation. The COG at the maximum load of $F_z(t) = -45.36\,\mathrm{kN}$ has been increased compared to the COG of case 1 ($\approx 0.07\,\mathrm{mm\,m^{-1}}$) by approximately 32 % for case 2 and 46 % for case 3, respectively. A COV can finally be calculated, e.g. of approximately 8 % at $F_z(t) = -45.36\,\mathrm{kN}$ considering Fig. 9b and 9d.

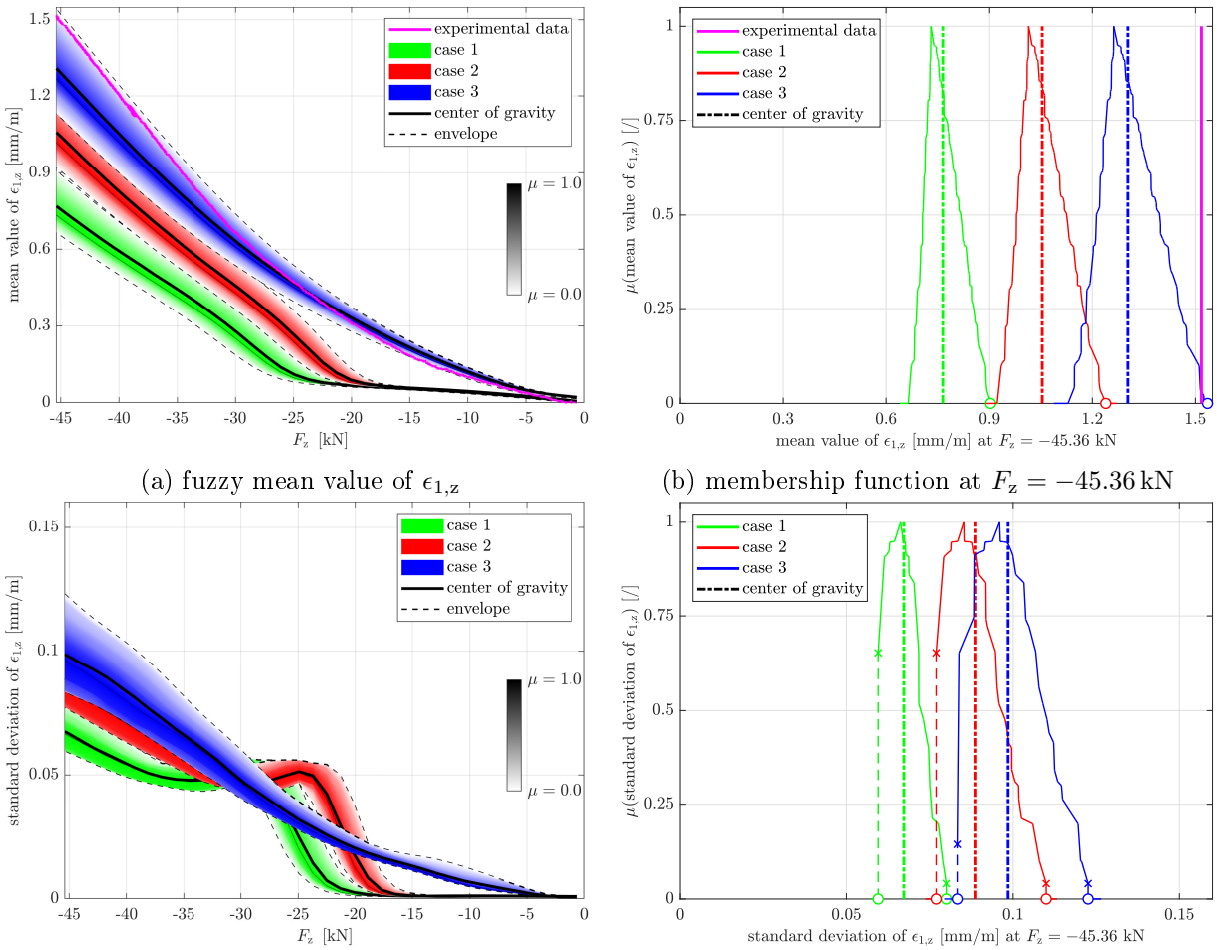

(a) fuzzy mean value of $\epsilon_{1,z}$

(b) membership function at $F_z = -45.36\,\mathrm{kN}$

(c) fuzzy standard deviation of $\epsilon_{1,z}$

(d) membership function at $F_z = -45.36\,\mathrm{kN}$

Figure 9: Fuzzy-stochastic output and experimental result for horizontal strain at position 1

5.2 Stereo optic camera system

The displacement fields just before failure are depicted in Fig. 10a during the experiment, in Fig. 10b for idea 1 and in Fig. 10c for idea 2. They are qualitatively quite similar. The maximum deflection is in the upper part of the web and the buckle is stretched in horizonal direction. For the numerical results, the COG of the fuzzy mean value has been visualized for all $\boldsymbol{x}$ at $F_z(t) = -45.36\,\mathrm{kN}$. The deviation of the two numerical results is shown in Fig. 10d. Generally, the values of idea 2 are higher than those of idea 1 in the upper part of the web by a maximum of 0.97 mm and lower in the lower part of the web by a maximum of 0.39 mm. Around the maximum deflection, the deviation between both ideas (compared to the displacement values) is negligible. In the experiment, the structure has collapsed then with an abrupt crack formation on the inside of the bottom of the upper flange.

The evaluation of the displacement in the center of the web $u_{\mathrm{M,norm}}$ is shown in Fig. 11a and 11b. Also here, the experimental curve is steeper than the numerical curves of case 1 and 2 and of case 3 for higher load values. The adjustments in case 2 and case 3 increase also the

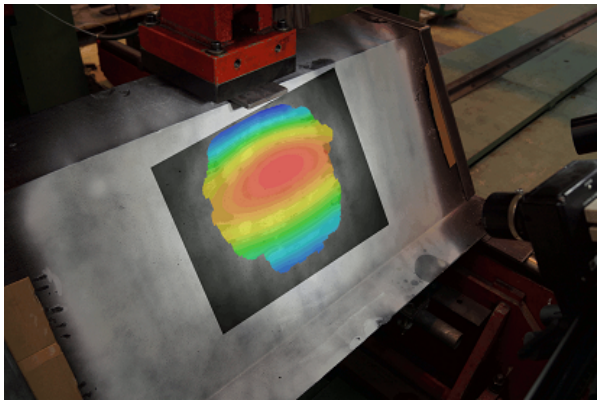

(a) experimental result

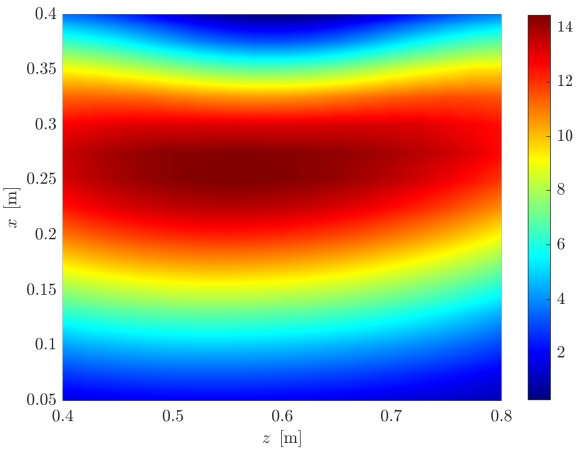

(b) **case 3/idea 1**: $\mathrm{COG}\left(\mu\left(\boldsymbol{u}_{\mathrm{norm}}\left(\boldsymbol{x}\right)\right)\right)$ [mm]

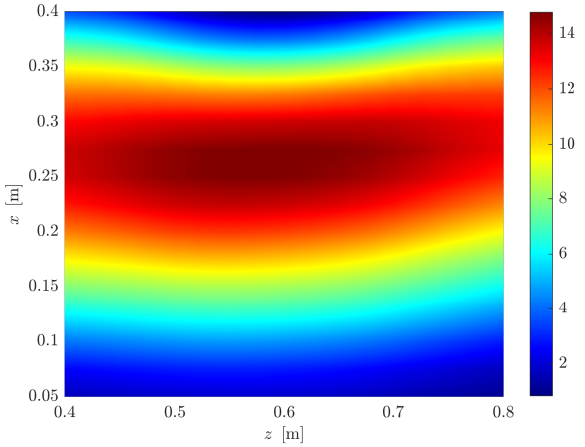

(c) **case 3/idea 2**: $\mathrm{COG}\left(\mu\left(\boldsymbol{u}_{\mathrm{norm}}\left(\boldsymbol{x}\right)\right)\right)$ [mm]

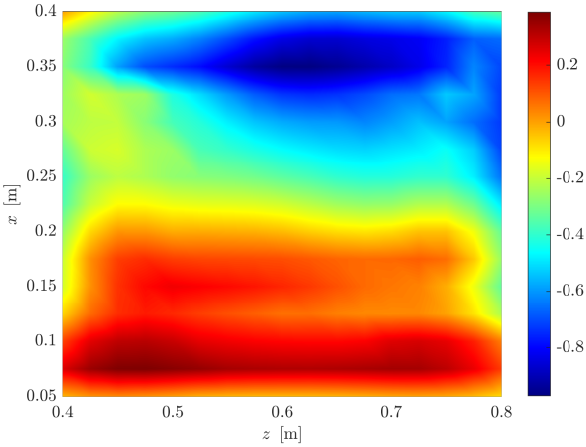

(d) **case 3**: Deviation of **idea 1** to **idea 2** [mm]

Figure 10: Displacements normal to web $\boldsymbol{u}_{\mathrm{norm}}\left(\boldsymbol{x}\right)$ just before failure at $F_{\mathrm{z}} = -45.36\,\mathrm{kN}$

displacement values, see Fig. 11a. The effect on $u_{\mathrm{M,norm}}$ of the pre-deformed geometry in case 3 is smaller than on $\epsilon_{1,\mathrm{z}}$, so the experimental curve is partly outside of the support of the fuzzy mean value for case 3, e.g. $19.51 \notin [12.24, 17.38]\,\mathrm{mm}$ at $F_{\mathrm{z}}\left(t\right) = -45.36\,\mathrm{kN}$.

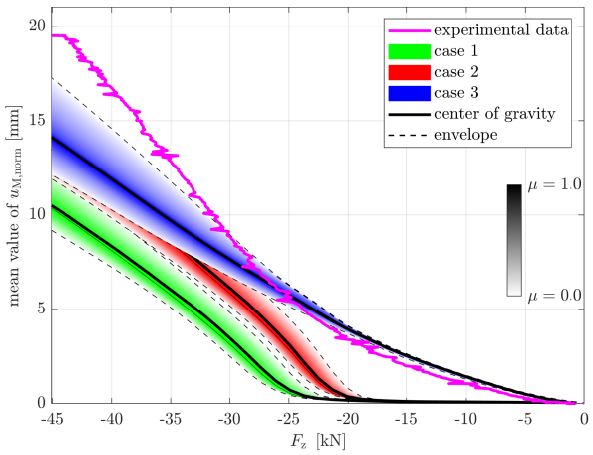

(a) fuzzy mean value of $u_{\mathrm{M,norm}}$

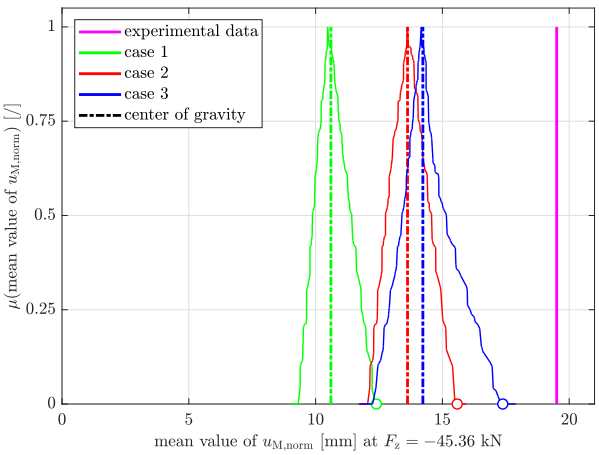

(b) membership function at $F_{\mathrm{z}} = -45.36\,\mathrm{kN}$

Figure 11: Fuzzy-stochastic output and experimental result for displacement normal to web

5.3 Sensitivity analysis

The system outcomes

$$\boldsymbol{y}\left(\boldsymbol{p}, F_{\mathrm{z}}\left(t\right), \boldsymbol{x}\right) = \begin{pmatrix} \epsilon_{1,\mathrm{z}}\left(\boldsymbol{p}, F_{\mathrm{z}}\left(t\right)\right) \\ \epsilon_{2,\mathrm{x}}\left(\boldsymbol{p}, F_{\mathrm{z}}\left(t\right)\right) \\ \epsilon_{3,\mathrm{z}}\left(\boldsymbol{p}, F_{\mathrm{z}}\left(t\right)\right) \\ \boldsymbol{u}_{\mathrm{norm}}\left(\boldsymbol{p}, F_{\mathrm{z}}\left(t\right), \boldsymbol{x}\right) \end{pmatrix} \tag{2}$$

depend on the uncertain parameters $\boldsymbol{p}$ and on spatial-temporal information. To understand the sensitivity of $\boldsymbol{y}$ from $\boldsymbol{p}$, a sensitivity analysis has been conducted resulting in the sensitivity matrix

$$\boldsymbol{G} = \left(\frac{\partial y_i}{\partial p_j}\right)_{i=1,\ldots,m;\ j=1,\ldots,n} = \begin{pmatrix} \frac{\partial y_1}{\partial p_1} & \frac{\partial y_1}{\partial p_2} & \cdots & \frac{\partial y_1}{\partial p_n} \\ \vdots & \vdots & \ddots & \vdots \\ \frac{\partial y_m}{\partial p_1} & \frac{\partial y_m}{\partial p_2} & \cdots & \frac{\partial y_m}{\partial p_n} \end{pmatrix} \tag{3}$$

For simplification purposes, the uncertainty has been excluded from $\boldsymbol{p}$ using and varying only the mean or core values, respectively. The evaluation of $\boldsymbol{y}$ has been conducted at $F_{\mathrm{z}}\left(t\right) = -45.36\,\mathrm{kN}$. In Fig. 12, the normalized output variables $(\epsilon_{1,\mathrm{z}}, u_{\mathrm{M,norm}})$ are exemplarily depicted for varying fiber volume content φ, web thickness t_{w}, stiffness in fiber direction $E_{\parallel\mathrm{f}}$ and offset of the upper flange Δ_{uf}.

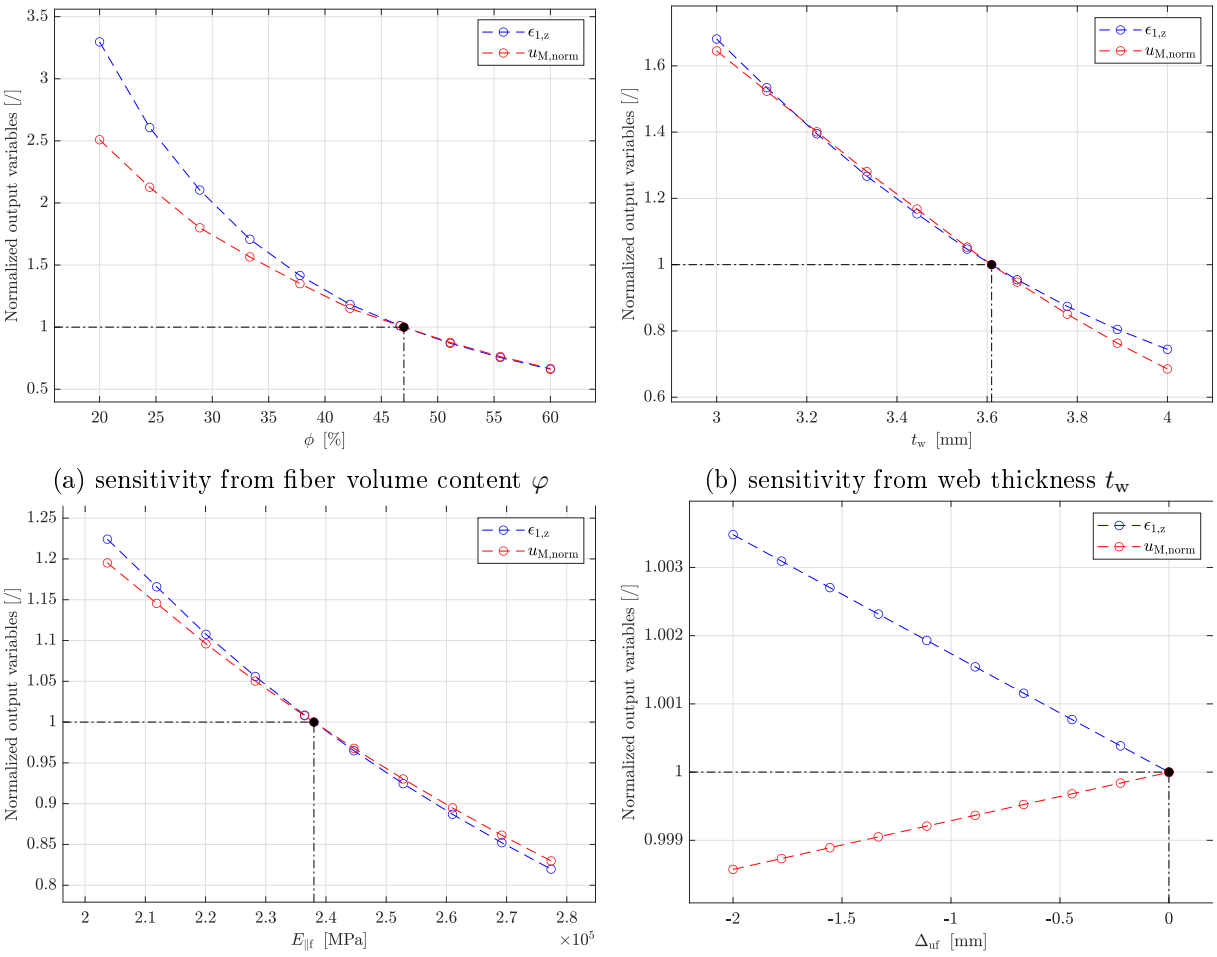

(a) sensitivity from fiber volume content φ

(b) sensitivity from web thickness t_{w}

(c) sensitivity from stiffness in fiber direction $E_{\parallel\mathrm{f}}$

(d) sensitivity from offset of the upper flange Δ_{uf}

Figure 12: sensitivity of $(\epsilon_{1,\mathrm{z}}, u_{\mathrm{M,norm}})$ at $F_{\mathrm{z}} = -45.36\,\mathrm{kN}$ from certain input variables

It has been determined that the system outcomes $\boldsymbol{y}$ are especially sensitive from the following parameters: φ, t_{w}, $E_{\parallel\mathrm{f}}$, $r_{\parallel}$ and u_{imp}. All of these parameters are influencing mainly the stiffness

of the tilted webs and the buckling behavior due to the applied vertical load $F_\mathrm{z}(t)$. The structural stiffness in fiber direction ($\|$) is more important than the stiffness in perpendicular direction ($\perp$). That means, that the material uncertainty in parameters like $E_{\perp\mathrm{f}}$, $G_{\perp\|\mathrm{f}}$, $\nu_{\perp\|\mathrm{f}}$, E_m and G_m is less important in this application. Furthermore, the geometrical deviations (see Fig. 12d for Δ_uf) and the uncertainties concerning the edge support area are present, but practically negligible. In the defined support with minimum and maximum values (see Section 4.3 and 4.4), the investigated system outcomes $(\epsilon_{1,\mathrm{z}}, u_{\mathrm{M,norm}})$ at $F_\mathrm{z}(t) = -45.36\,\mathrm{kN}$ are only varying with $\pm 5\%$ around the value determined by using the mean or core values, respectively.

6 Conclusions

In the present study, the global stability failure of a three-dimensional composite structure in the presence of unavoidable polymorphic uncertainties is investigated numerically as well as experimentally. The structure is a thin-walled carbon fiber reinforced shell with an omega cross-section. The shell has been manufactured, measured and loaded until failure in a symmetric three-point bending test. The measured uncertainties are incorporated in the numerical model by stochastic variables. Other uncertainties are only vaguely given for which fuzzy variables have been used. To overcome the computational costs, a surrogate modeling is essential. Individual ANNs could be founded by the use of the hyperband algorithm and a following grid search for various system outcomes like strains and displacements. Small training and validation loss values confirm the application of ANNs for the numerical spatial-temporal prediction.

The experimental results could be reflected qualitatively, but quantitative deviations are still present. The experimental curves are mostly steeper than the numerical ones. For all three numerically investigated cases, the output fuzzy standard deviations are approximately 8 % of the output fuzzy mean values by what the influence of the stochastic input parameters becomes visible. The influence of the fuzzy input parameters can be seen for example in the support intervals of the output fuzzy mean values, which are approximately $-13\,\%/+18\,\%$ around the associated COGs. The reduction of the fiber volume content from 55 % to 47 % in case 2 decreases the stiffness of the structure and decreases the deviation to the experimentally determined strains and displacements. In addition, the pre-deformation according to the symmetrical buckling mode in case 3 decreases the deviation once more and the experimental curve can be better retraced, especially for smaller load values.

The finally conducted sensitivity analysis shows that the fiber volume content, the structural thicknesses and the stiffness in fiber direction influence the investigated system outcomes the most. Uncertainties in other parameters, especially the material densities, the stiffness parameters perpendicular to the fiber direction or the global geometrical deviations can be neglected for the investigated system outcomes.

Acknowledgements

The authors gratefully acknowledge the financial support of the German Research Foundation (DFG) within the Subproject 4 (312928137) of the Priority Programme "Polymorphic uncertainty modelling for the numerical design of structures – SPP 1886".

References

[1] A. Y. Alanis, N. Arana-Daniel, and C. López-Franco, editors. *Artificial Neural Networks for Engineering Applications*. Academic Press, 2019.

[2] K. Bathe. *Finite Element Procedures*. Number 2 in Finite Element Procedures. Prentice Hall, 2014.

[3] P. Brøndsted and R. Nijssen, editors. *Advances in wind turbine blade design and materials*. Number 47 in Woodhead Publishing Series in Energy. Woodhead Publishing, 2013.

[4] J. Cao, D. Farnham, and U. Lall. Spatial-temporal wind field prediction by artificial neural networks. *ArXiv*, abs/1712.05293, 2017.

[5] S. G. Castro, R. Zimmermann, M. A. Arbelo, R. Khakimova, M. W. Hilburger, and R. Degenhardt. Geometric imperfections and lower-bound methods used to calculate knock-down factors for axially compressed composite cylindrical shells. *Thin-Walled Structures*, 74:118–132, 2014.

[6] F. Chollet et al. Keras. https://keras.io, 2015.

[7] A. K. Ditcher, F. E. Rhodes, and J. P. H. Webber. Non-linear stress-strain behaviour of carbon fibre reinforced plastic laminates. *The Journal of Strain Analysis for Engineering Design*, 16(1):43–51, 1981.

[8] M. Drieschner, L. Eichner, F. Seiffarth, and Y. Petryna. PolyUQ: framework for solving problems with polymorphic uncertainties. Preprint Technische Universität Berlin, 2021.

[9] G. E. Erten, S. B. Keser, and M. Yavuz. Grid search optimised artificial neural network for open stope stability prediction. *International Journal of Mining, Reclamation and Environment*, 35(8):600–617, 2021.

[10] W. Flügge. *Die Stabilität der Kreiszylinderschale*, volume 3. Springer-Verlag, 1932.

[11] S. Freitag, P. Edler, K. Kremer, and G. Meschke. Surrogate modelling for solving optimization problems with polymorphic uncertain data. In *Proceedings of the 8th International Workshop on Reliable Engineering Computing (REC 2018)*, pages 31–39, 2018.

[12] I. J. Goodfellow, Y. Bengio, and A. Courville. *Deep Learning*. MIT Press, Cambridge, MA, USA, 2016.

[13] M. Götz, W. Graf, and M. Kaliske. Structural design with polymorphic uncertainty models. 9:112–131, 2015.

[14] W. Graf, S. Freitag, J.-U. Sickert, and M. Kaliske. Structural analysis with fuzzy data and neural network based material description. *Computer-Aided Civil and Infrastructure Engineering*, 27(9):640–654, 2012.

[15] M. Hanss. *Applied Fuzzy Arithmetic: An Introduction with Engineering Applications*. Springer-Verlag Berlin Heidelberg, 1st edition, 2005.

[16] ISO. *Development of Fibre-Reinforced Plastics components - Analysis (2014-3)*. Beuth Verlag GmbH, Berlin, 2006.

[17] R. Khakimova, S. G. Castro, D. Wilckens, K. Rohwer, and R. Degenhardt. Buckling of axially compressed cfrp cylinders with and without additional lateral load: Experimental and numerical investigation. *Thin-Walled Structures*, 119:178–189, 2017.

[18] A. D. Kiureghian and O. Ditlevsen. Aleatory or epistemic? does it matter? *Structural Safety*, 31(2):105–112, 2009. Risk Acceptance and Risk Communication.

[19] A. Krizhevsky, I. Sutskever, and G. E. Hinton. Imagenet classification with deep convolutional neural networks. *Commun. ACM*, 60(6):84–90, 2017.

[20] W. V. Leekwijck and E. E. Kerre. Defuzzification: criteria and classification. *Fuzzy Sets and Systems*, 108(2):159–178, 1999.

[21] L. Li, K. Jamieson, G. DeSalvo, A. Rostamizadeh, and A. Talwalkar. Hyperband: A novel bandit-based approach to hyperparameter optimization. *Journal of Machine Learning Research*, 18(185):1–52, 2018.

[22] I. Papaioannou, M. Daub, M. Drieschner, F. Duddeck, M. Ehre, L. Eichner, M. Eigel, M. Götz, W. Graf, L. Grasedyck, R. Gruhlke, D. Hömberg, M. Kaliske, D. Moser, Y. Petryna, and D. Straub. Assessment and design of an engineering structure with polymorphic uncertainty quantification. *GAMM-Mitteilungen*, 42(2):e201900009, 2019.

[23] F. Pedregosa, G. Varoquaux, A. Gramfort, V. Michel, B. Thirion, O. Grisel, M. Blondel, P. Prettenhofer, R. Weiss, V. Dubourg, J. Vanderplas, A. Passos, D. Cournapeau, M. Brucher, M. Perrot, and E. Duchesnay. Scikit-learn: Machine learning in Python. *Journal of Machine Learning Research*, 12:2825–2830, 2011.

[24] E. Pimenidis and C. Jayne. *Engineering Applications of Neural Networks: 19th International Conference, EANN 2018, Bristol, UK, September 3-5, 2018, Proceedings*. Springer Publishing Company, Incorporated, 1st edition, 2018.

[25] R&G Faserverbundstuffe GmbH. *Technische Daten Epoxidharz L 20*, 2010.

[26] R. Rojas. *Neural Networks: A Systematic Introduction*. Springer-Verlag, Berlin, Heidelberg, 1996.

[27] F. N. Schietzold, A. Schmidt, M. M. Dannert, A. Fau, R. M. N. Fleury, W. Graf, M. Kaliske, C. Könke, T. Lahmer, and U. Nackenhorst. Development of fuzzy probability based random fields for the numerical structural design. *GAMM-Mitteilungen*, 42(1):e201900004, 2019.

[28] H. Schürmann. *Konstruieren mit Faser-Kunststoff-Verbunden*. VDI-Buch. Springer-Verlag Berlin Heidelberg, 2007.

[29] Teijin Carbon Europe GmbH. *Produktprogramm und Eigenschaften für Tenax® STS Filamentgarn*, 2010.

[30] A. Vanaerschot, S. V. Lomov, D. Moens, and D. Vandepitte. Variability in composite materials properties. In *Uncertainty in Mechanical Engineering II*, volume 807 of *Applied Mechanics and Materials*, pages 23–33. Trans Tech Publications Ltd, 2015.

[31] E. Verwimp, T. Tysmans, M. Mollaert, and S. Berg. Experimental and numerical buckling analysis of a thin trc dome. *Thin-Walled Structures*, 94:89–97, 2015.

[32] Z. Waszczysznk, editor. *Neural Networks in the Analysis and Design of Structures*. Number 404 in CISM International Centre for Mechanical Sciences. Springer-Verlag Wien, 1999.

[33] C. Wolf. Messtechnische Erfassung und Modellierung von Imperfektionen und Stabilität dünnwandiger CFK-Bauteile. Master's thesis, Techische Universität Berlin, 2019.

[34] D. Xu, J. Huang, Y. Zhang, H. Cheng, and S. Zhang. Dependency of statistical correlation between ply elastic properties of FRP. *IOP Conference Series: Materials Science and Engineering*, 774:012121, 2020.

[35] A. Ziat, E. Delasalles, L. Denoyer, and P. Gallinari. Spatio-temporal neural networks for space-time series forecasting and relations discovery. In *2017 IEEE International Conference on Data Mining (ICDM)*, pages 705–714, 2017.